Constructing 2D Curve Atlases

Thomas B. Sebastian
Div. of Engineering
Brown University
Providence RI 02912

Joseph J. Crisco
Dept. of Orthopedics
Rhode Island Hospital
Providence, RI 02903

Philip N. Klein
Dept. of Computer Science
Brown University
Providence RI 02912

Benjamin B. Kimia
Div. of Engineering
Brown University
Providence RI 02912

Abstract

We present an approach to computing a curve atlas based on deriving a correspondence between two curves. This correspondence is based on a notion of an alignment curve *and on a measure of similarity between the intrinsic properties of the curve, namely, length and curvature. The optimal correspondence is found by an efficient dynamic-programming method. This is then used to compute an average for a set of curves and applied to computing the averages of bone shapes and corpus callosum as examples, towards constructing a computational atlas. The proposed notion of alignment also leads to a registration method, which is illustrated with several examples.*

1 Introduction

This paper presents a method to construct the average of 2D shape outlines (curves) using their intrinsic properties. A computational framework for constructing an average curve and for characterizing the deviations from the average has a wide variety of applications in medical imaging. For example, in comparing the anatomy of a sample medical structure to a population of similar structures, the average curve represents the average anatomy. This can be used for measuring differences in anatomy between diseased/healthy, male/female populations, and across a range of ages. Correlating "abnormal" deviations from the average anatomy with diseased states can potentially lead to diagnostic measures. The current clinical language for describing "abnormal" shape is limited to a simple set of measurements in the form of simple functions of length, areas, volumes, etc [15].

A number of recent approaches have jointly led to the emergence of the field of "computational neuroanatomy" [10], with the goal of capturing the average shape of medical structures of interest and quantifying free-form variations. Bookstein [4] uses a thin-plate spline method based on landmarks to compare the shape of corpus callosum in the human brains. Pizer *et al.* [9] have proposed the "deformable shape loci" model that represents the shape as a graph of boundary and medialness points. Shape differences are then measured as the squared distance of the properties of the links. Davatzikos *et al.* [7] have proposed an interesting two-step approach for deforming brain images. First, a one-to-one correspondence between points on the boundaries of the two images is computed, and in the second step an elastic warping is done so that the corresponding points are aligned. This approach assumes that the correspondence between boundary points can be found by uniform scaling and and bending, which can fail in "abnormal" brains. Taylor *et al.* [16] use "Active Shape Models" which represent the shape as a mean (average) shape plus a set of linearly independent variation modes that are derived using a training set. These models are effective in a variety of applications [16]. However, they do not adequately represent low frequency (for $e.g.$, diseased) states. Christensen *et al.* [12] superimpose an extrinsic coordinate system on the anatomy and model its displacement field to capture shape variations of human brains. They use the images generated from a normal subject as the anatomical "textbook", and compute the transformation required to deform the textbook into the images of the other subjects. Average anatomy is then computed by applying the average transformation to the textbook. This approach penalizes large deformations, and is not suitable for images that are very different. Bakircioglu *et al.* [1] have proposed to match brain surfaces by matching the Frenet distances of extremal curvature lines. The curve matching is restricted to be diffeomorphic, which rules out deletion of a curve segment, necessary in modeling diseased state.

Another important application of curve matching in medical imaging is tracking the motion of anatomical structures. Duncan *et al.* [8] and Cohen *et al.* [5] have used a bending energy minimization method to track the left ventricular endocardial motion and mitral valve, respectively. See Younes [18] for a similar approach. Tagare *et al.* [17], point out the inherent asymmetry of the above approaches, and propose a symmetric method which penalizes differences in local orientation for tracking left ventricle in diastole and systole.

Our approach to computing the average shape of 2D outlines (curves) is based on using the *intrinsic* properties of the outlines as follows. First, the optimal alignment between two curves is defined based on the intrinsic properties of the curves, Section 2. Second, the average curve is computed by averaging the corresponding segments on the two curves, using the optimal alignment between the two curves, Section 3. The correspondence between the curves is also be used to register curves, *i.e.*, to recover the transformation parameters (translation vector, rotation angle and global scaling) of the two curves, Section 4. Section 5 discusses how the average outline of the radius bone of male and female subjects can be compared.

2 Curve Matching

This section discusses the problem of matching and aligning two curves $\mathcal{C}(s) = (x(s), y(s))$, $s \in [0, L]$ and $\bar{\mathcal{C}}(\bar{s}) = (\bar{x}(\bar{s}), \bar{y}(\bar{s}))$, $\bar{s} \in [0, \bar{L}]$, where s is arc length, x and y are coordinates of each point, L is length, and each is similarly defined for $\bar{\mathcal{C}}$. A central premise of this approach is that the "goodness" of the optimal match is the sum of "goodness" of the optimal matches between two corresponding subsegments. This allows an energy functional to convey the goodness of a match as a function of the correspondence or alignment of the two curves [5, 18, 7]. Let a mapping g,

$$g : [0, L] \to [0, \bar{L}], \qquad g(s) = \bar{s},$$

represent an alignment of the two curves. Cohen *et al.* [5] use "bending" and "stretching" energies in a physical analogy similar to the one used in formulating active contours or snakes [11]. Specifically, they compare the displacement velocities and bending energies in the form of

$$\mu[g] = \int_{\mathcal{C}} \left| \frac{\partial}{\partial s} (\bar{\mathcal{C}}(\bar{s}) - \mathcal{C}(s)) \right|^2 ds + R \int_{\mathcal{C}} (\kappa_{\mathcal{C}}(s) - \kappa_{\bar{\mathcal{C}}}(\bar{s}))^2 ds,$$

where κ is the curvature along the curves and $\bar{s} = g(s)$. Younes [18] uses a similar functional which measures the variation in the displacement vector ($\overrightarrow{\mathcal{C}\bar{\mathcal{C}}}$), leading to

$$\mu[g] = \int_{\mathcal{C}} (g_s - 1)^2 ds + \int_{\mathcal{C}} (\bar{\theta}(\bar{s}) \circ g(s) - \theta(s))^2 ds,$$

where θ and $\bar{\theta}$ are the angles that the curves $\mathcal{C}$ and $\bar{\mathcal{C}}$ make with the horizontal axis, respectively. Both these approaches are not invariant to the rotation of one curve with respect to the other, and hence the optimal orientation must be found as well. In addition, Cohen's method is not invariant to sampling. We address both these issues below, but first define some notation.

Definition: Let $\mathcal{C}\big|_{[s_1, s_2]}$ denote the portion of the curve from s_1 to s_2 and $g\big|_{([s_1, s_2], [\bar{s}_1, \bar{s}_2])}$ the restriction of the mapping g to $[s_1, s_2]$. Define a measure μ on this alignment
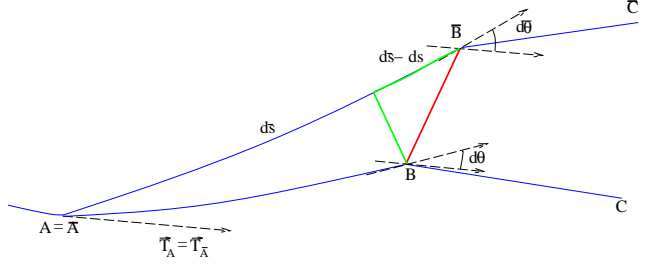

Figure 1. The cost of deforming an infinitesimal segment AB to segment $\bar{A}\bar{B}$, when the initial points and the initial tangents are aligned ($A = \bar{A}$, $\vec{T}_A = \vec{T}_{\bar{A}}$), is related to the distance $B\bar{B}$, and is defined by $|d\bar{s} - ds| + R|d\bar{\theta} - d\theta|$.

function,

$$\mu[g]\big|_{([s_1, s_2], [\bar{s}_1, \bar{s}_2])} : g\big|_{([s_1, s_2], [\bar{s}_1, \bar{s}_2])} \to \mathbf{R}^+,$$

which is inversely proportional to the goodness of the match, *i.e.*, it denotes the cost of deforming $\mathcal{C}\big|_{[s_1, s_2]}$ to $\bar{\mathcal{C}}\big|_{[\bar{s}_1, \bar{s}_2]}$.

We restrict this measure μ to one which satisfies an *additivity property*

$$\mu[g]\big|_{([s_1, s_3], [\bar{s}_1, \bar{s}_3])} = \mu[g]\big|_{([s_1, s_2], [\bar{s}_1, \bar{s}_2])} + \mu[g]\big|_{([s_2, s_3], [\bar{s}_2, \bar{s}_3])},$$
$$\forall s_1 \le s_2 \le s_3 \in [0, L], \bar{s}_1 \le \bar{s}_2 \le \bar{s}_3 \in [0, \bar{L}]. \tag{1}$$

so that we can decompose the match process into a number of smaller matches and write it as a functional

$$\mu[g]\big|_{([0, L], [0, \bar{L}])} = \int_0^L \mu[g]\big|_{([s, s+ds][g(s), g(s+ds)])} ds \tag{2}$$

Then, the optimal match is given by

$$g^* = \operatorname*{argmin}_g \mu[g]\big|_{([0, L], [0, \bar{L}])}.$$

Definition: Let the distance between the two curves $\mathcal{C}$ and $\bar{\mathcal{C}}$ be defined as the cost of the optimal alignment of the two curves.

$$d(\mathcal{C}, \bar{\mathcal{C}}) = \mu(g^*).$$

Remark: It is clear that the distance function satisfies the following *suboptimal property* for $\bar{s}_i = g^*(s_i)$, $i = 1, 2, 3$,

$$d(\mathcal{C}\big|_{[s_1, s_3]}, \bar{\mathcal{C}}\big|_{[\bar{s}_1, \bar{s}_3]}) = d(\mathcal{C}\big|_{[s_1, s_2]}, \bar{\mathcal{C}}\big|_{[\bar{s}_1, \bar{s}_2]}) + d(\mathcal{C}\big|_{[s_2, s_3]}, \bar{\mathcal{C}}\big|_{[\bar{s}_2, \bar{s}_3]}). \tag{3}$$

Consider two infinitesimal curve segments of $\mathcal{C}$ (AB) and $\bar{\mathcal{C}}$ ($\bar{A}\bar{B}$) of lengths ds, $d\bar{s}$ and curvatures κ, $\bar{\kappa}$, respectively. Since we only compare the intrinsic aspects of the curves, we can align these two curves so that A and $\bar{A}$ coincide, as well as tangents at A and $\bar{A}$, $\vec{T}_A$ and $\vec{T}_{\bar{A}}$, respectively, Figure 1. The cost of matching the curve segments is related to the distance $B\bar{B}$, which we define as

$$\mu[g]\big|_{([s_1, s_2], [\bar{s}_1, \bar{s}_2])} = |d\bar{s} - ds| + R|d\bar{\theta} - d\theta|, \tag{4}$$

where R is a constant related to the average size of ds. Then, the resulting functional is given by

$$
\begin{aligned}
\mu[g] &= \int_{\mathcal{C}} \left[\left| \frac{d\bar{s}}{ds} - 1 \right| + R \left| \frac{d\bar{\theta}(\bar{s})}{d\bar{s}} \frac{d\bar{s}}{ds} - \frac{d\theta(s)}{ds} \right| \right] ds \\
&= \int_{\mathcal{C}} \left[|g' - 1| + R |\bar{\kappa}(\bar{s}) g(s) - \kappa(s)| \right] ds
\end{aligned}
\tag{5}
$$

The first term in the functional penalizes "stretching" while the second term penalizes "bending". However, this formulation of the curve matching problem is inherently asymmetric. This is similar to the objection raised by Tagare *et al.* [17] to algorithms which are based on differentiable function of one curve to the other. They instead propose a "bimorphism", which diffeomorphically maps a pair of curves to be matched, and correspond to a closed curve in space of $\mathcal{C}_1 \times \mathcal{C}_2$. They formulate a cost function that minimizes differences in local orientation change $|d\bar{\theta} - d\theta|$ along each differential segment of this curve, and seek a pair of functions ϕ_1 and ϕ_2, elements of the bimorphism, which optimize this cost functional. Note that, Tagare *et al.*'s [17] cost functional does not penalize stretching. This is problematic when handling with curves with differing topology, as in "abnormal" or diseased states.

We approach this asymmetry issue in a similar fashion. We note that the formulation allows for mapping an entire segment of the first curve to a single point in the second curve, but it is not possible to map a single point in the first curve to a segment in the second curve. This is because the notion of an alignment is captured by a (uni-valued) function g. To alleviate this difficulty we revise the formulation. Reconsider an alignment between two curves as a pairing of two particles, one on each curve traversing their respective paths monotonically, but with finite stops allowed. Let the alignment be specified in terms of two functions h and $\bar{h}$ relating arc length along $\mathcal{C}$ and $\bar{\mathcal{C}}$ to the newly defined curve parameter ξ, *i.e.*, $s = h(\xi)$, and $\bar{s} = \bar{h}(\xi)$. In cases where h is invertible, we have $\bar{s} = \bar{h}(h^{-1}(s)) = \bar{h} \circ h^{-1}(s)$, which allows for the use of an alignment function, $g = \bar{h} \circ h^{-1}$, as before. However, when h is not invertible, *i.e.*, when the first particle stops along the first curve for some finite time, g is not defined. While this formulation allows for a symmetric treatment of the curves, note that a superfluous degree of freedom is introduced as in [17], because different traversals h and $\bar{h}$ may give rise to the same alignment. While Tagare *et al.* [17] treat this degree of redundancy in the optimization involving two functions, we remove this additional degree of redundancy by considering the notion of an *alignment curve*, α, with coordinates h and $\bar{h}$

$$
\alpha(\xi) \triangleq (h(\xi), \bar{h}(\xi)), \ \xi \in [0, \tilde{L}], \ \alpha(0) = (0, 0), \ \alpha(\tilde{L}) = (L, \bar{L}),
$$

where ξ is the arc length along the alignment curve and $\tilde{L}$ is its length. The alignment curve can now be specified by a single function, namely, $\psi(\xi), \xi \in [0, \tilde{L}]$, where ψ denotes
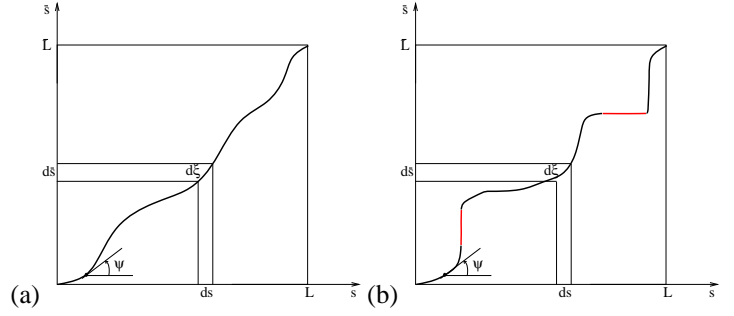

Figure 2. The alignment curve allows for a finite segment from one curve to be aligned with a single point on one curve, thus allowing for (b) the curve segment deletion or addition.

the angle between the tangent to the curve and the x-axis. The coordinates can then be obtained by integration

$$
h(\xi) = \int_0^{\xi} \cos(\psi(\eta)) d\eta, \ \bar{h}(\xi) = \int_0^{\xi} \sin(\psi(\eta)) d\eta, \ \xi \in [0, \tilde{L}].
$$

Note that ψ is constrained by monotonicity ($h' \geq 0$ and $\bar{h}' \geq 0$) to lie in $[0, \frac{\pi}{2}]$. The alignment between $\mathcal{C}$ and $\bar{\mathcal{C}}$ is then fully represented by single function ψ.

The goodness of the match corresponding to the alignment curve can now be rewritten in terms of ψ. First, if $h' \neq 0$ and $\bar{h}' \neq 0$ for $\xi \in [\xi_1, \xi_2]$, then $g = \bar{h} \circ h^{-1}$ is well defined and we rewrite $\mu[\psi]$ in terms of g using Equations 2 and 4,

$$
\begin{aligned}
\mu(\psi)\big|_{[\xi_1, \xi_2]} &= \int_{\xi_1}^{\xi_2} \mu[\bar{h} \circ h^{-1}]\Big|_{([h(\xi), h(\xi+d\xi)], [\bar{h}(\xi), \bar{h}(\xi+d\xi)])} d\xi \\
&= \int_{\xi_1}^{\xi_2} \left| \frac{dh}{d\xi} - \frac{d\bar{h}}{d\xi} \right| + R \left| \frac{d\theta}{d\xi} - \frac{d\bar{\theta}}{d\xi} \right| d\xi \\
&= \int_{\xi_1}^{\xi_2} \left| \frac{dh}{d\xi} - \frac{d\bar{h}}{d\xi} \right| + R \left| \frac{d\theta}{ds} \frac{ds}{d\xi} - \frac{d\bar{\theta}}{d\bar{s}} \frac{d\bar{s}}{d\xi} \right| d\xi \\
&= \int_{\xi_1}^{\xi_2} |\cos(\psi) - \sin(\psi)| + \\
&\quad\quad R |\kappa(h) \cos(\psi) - \bar{\kappa}(\bar{h}) \sin(\psi)| d\xi
\end{aligned}
\tag{6}
$$

Second, consider that one of h' or $\bar{h}'$ is zero at a point, say $h'(\xi) = 0$, implying that this point maps to a corresponding interval $[\bar{h}(\xi), \bar{h}(\xi + d\xi)]$. The cost of mapping the point $h(\xi)$ to the interval $[\bar{h}(\xi), \bar{h}(\xi + d\xi)]$ is defined by enforcing continuity of the cost with deformations: consider the cost of aligning the interval $[h(\xi), h(\xi + d\xi)]$ to the interval $[\bar{h}(\xi), \bar{h}(\xi+d\xi)]$ as the first interval shrinks to a point, *i.e.*, as $\psi \to \frac{\pi}{2}$. In this case, the energy in Equation 6 can be used in the limiting case $\psi \to \frac{\pi}{2}$, or $\cos(\psi) \to 0$. Similarly, the case where an interval in the first curve is mapped to a point in the second curve, is the limiting case of $\psi \to 0$ or $\sin(\psi) \to 0$, and Equation 6 can again be used. Thus, the overall cost of the alignment ψ is well defined in all cases

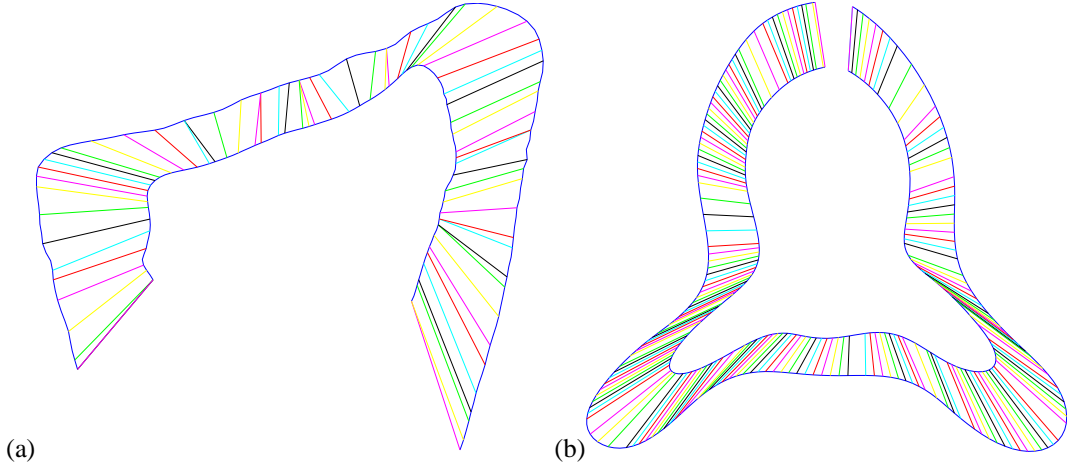(a)   (b)

Figure 4. Two examples of the optimal correspondence between the profiles of the radius bone in the sagittal direction (a) and a vertebra of the spine in the axial direction (b) of two subjects obtained using the curve matching algorithm, Section 2. The curves being matched (shown in blue) were segmented manually from CT images. The original spine images were obtained from the Visible Human Data Set from the National Library of Medicine. One of the curve has been scaled to display the match lines (randomly colored lines) better.
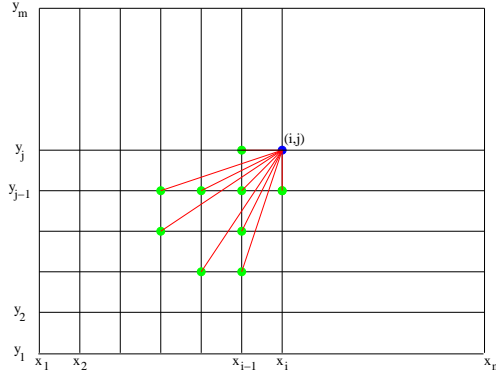

Figure 3. This figure illustrates the template that is used to in the Dynamic Programming implementation of Equation 7. The entry at (i, j) is the cost to match the curve segments $x_1, x_2, \ldots, x_i$ and $y_1, y_2, \ldots, y_j$ $d(i, j)$. To update the cost at (i, j) (blue dot) we limit the choices of the k and l in Equation 8, so that only costs at the a limited set of points (green dots) are considered.

of Equation 6,

$$\mu[\psi] = \int_0^{\tilde{L}} \big[|\cos(\psi) - \sin(\psi)| \\ + R|\kappa(h)\cos(\psi) - \bar{\kappa}(\bar{h})\sin(\psi)| \big] d\xi, \tag{7}$$

subject to the following constraints

$$0 \le \psi \le \frac{\pi}{2}, \int_0^{\tilde{L}} \cos(\psi) d\xi = L, \text{ and } \int_0^{\tilde{L}} \sin(\psi) d\xi = \bar{L}.$$

Algorithm: We minimize the above functional by a dynamic-programming method [2, 6]. Let the curves $\mathcal{C}$ and $\bar{\mathcal{C}}$ be discretized at samples $x_1, x_2, \ldots, x_n$ and $y_1, y_2, \ldots, y_m$, respectively, Figure 3. These are samples

along h and $\bar{h}$, the axes in Figure 2. Let $d(i, j)$ denote the cost of matching the curve segments $x_1, x_2, \ldots, x_i$ and $y_1, y_2, \ldots, y_j$ and let $\delta([k, i], [l, j])$ be the cost of matching the segments $x_k, \ldots, x_i$ and $y_l, \ldots, y_j$. Then, a discrete version of Equation 3 can be written as

$$d(i, j) = \min_{k, l} \big[d(i - k, j - l) + \delta([i - k, i], [j - l, j]) \big]. \tag{8}$$

We discretize ψ, as a first approximation, to nine values achieved by using a small template (shown in Figure 3). This template limits the choices of the k and l.

We have applied the curve matching to a few medical imaging applications, with good results. Figure 4(a) shows the optimal matching for the profiles of the radius bone of the wrist taken in the sagittal direction. Figure 4 shows the optimal matching for the outline of a pair of vertebra of the spine taken in the axial direction.

3 Curve Averaging

This section discusses the computation of the "average" curve. Given N curves, $\mathcal{C}_1, \mathcal{C}_2, \ldots, \mathcal{C}_N$, the goal is to compute the average curve $\hat{\mathcal{C}}$ which is the curve that minimizes $\sum_{i=1}^{N} d^2(\mathcal{C}_i, \hat{\mathcal{C}})$. This requirement is rather stringent in that it should hold for all curves segments $\mathcal{C}\big|_{[S_i, S_i + \Delta S_i]}$ of $\mathcal{C}_i$ aligned with the curve segment $\hat{\mathcal{C}}\big|_{[\hat{s}, \hat{s} + \Delta \hat{s}]}$. Ideally, we must seek a curve $\hat{\mathcal{C}}$ such that for any $\hat{s}$ and $\Delta \hat{s}$ the infinitesimal curve segment $\bar{\mathcal{C}}\big|_{[\hat{s}, \hat{s} + \Delta \hat{s}]}$ is the result of averaging the corresponding curve segments $\mathcal{C}_i\big|_{[s_i, s_i + \Delta s_i]}$. Given the curve $\hat{\mathcal{C}}$, it is not difficult to compute the corresponding segments on $\mathcal{C}_i$, as shown in Section 2. However, when $\hat{\mathcal{C}}$ is
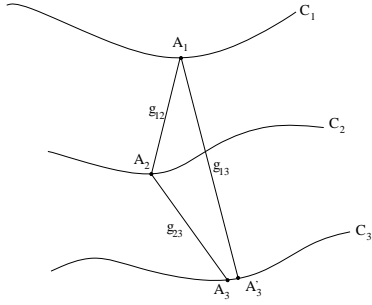
Figure 5. The dilemma in averaging curves is that optimal alignments are not transitive: For an arbitrary point $A_1 \in \mathcal{C}_1$, its optimal match $A_2 \in \mathcal{C}_2$, the optimal match of A_2 on $\mathcal{C}_3$, A_3, is not the same as the optimal match of A_1 on $\mathcal{C}_3$, A_3'.
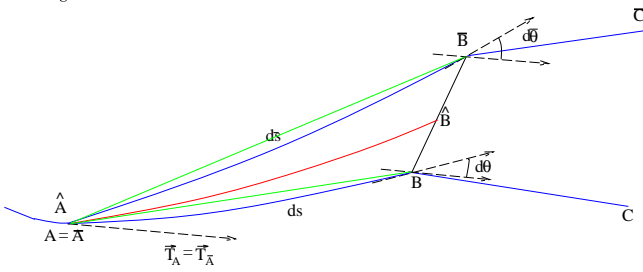

Figure 6. The average segment $\hat{A}\hat{B}$ of two curve segments AB and $\bar{A}\bar{B}$, when the initial points and the initial tangents are aligned ($A = \bar{A}$, $\vec{T}_A = \vec{T}_{\bar{A}}$), is computed by averaging the endpoints.

not available, this becomes a computationally intractable problem. The computation is made difficult by the fact that the alignment property is not transitive, Figure 5. The computational problem of finding $\hat{\mathcal{C}}$ and the alignments simultaneously is rather intractable. Rather, we select one of the curves, say $\mathcal{C}_1$ as a "reference curve" and average for s_1 and Δs_1, $\mathcal{C}_1|_{[s_1, s_1 + \Delta s_1]}$ and the corresponding segment $\mathcal{C}_2|_{[s_2, s_2 + \Delta s_2]}$ to define the corresponding average $\hat{\mathcal{C}}|_{[\hat{s}, \hat{s} + \Delta \hat{s}]}$.[1]

Consider then the case of averaging two corresponding segments AB and $\bar{A}\bar{B}$ as in Figure 1. Since only the intrinsic properties are significant, let A and $\bar{A}$ coincide. Then, computation of $\hat{A}$ is straightforward, $\hat{A} = A = \bar{A}$. Since, $B\bar{B}$ is the main indicator of distance between these two curve segments, $\hat{B}$ is computed by averaging the end points B, and $\bar{B}$. To compute an intrinsic average of the endpoints, we express the endpoints in terms of the initial point and the length and relative orientation of the segments. Currently, we use a linear approximation for the curve segments to

---

[1]As before, we demand that the averaging process be invariant to rotation and translation of the curves with respect to one another. In other words, if $\hat{\mathcal{C}}$ is the average of two curves $\mathcal{C}$ and $\bar{\mathcal{C}}$, then the average curve of C and a transformed version of $\bar{\mathcal{C}}$ is also $\hat{\mathcal{C}}$ up to a global rotation/translation. This implies that the averaging of the infinitesimal pieces has to be done using the intrinsic properties of the curves.

compute the average curve. We could use a higher order model if the need arises. Specifically, the endpoints can be written as

$$B = A + (ds \cos(d\theta), ds \sin(d\theta)), \quad \bar{B} = \bar{A} + (d\bar{s} \cos(d\bar{\theta}), d\bar{s} \sin(d\bar{\theta}))$$

Then, the average is computed as

$$\hat{B} = \hat{A} + \left(\frac{ds \cos(d\theta) + d\bar{s} \cos(d\bar{\theta})}{2}, \frac{ds \sin(d\theta) + d\bar{s} \sin(d\bar{\theta})}{2} \right)$$

with $d\hat{s} \cos(d\hat{\theta}) = \dfrac{ds \cos(d\theta) + d\bar{s} \cos(d\bar{\theta})}{2}$ and $d\hat{s} \sin(d\hat{\theta}) = \dfrac{ds \sin(d\theta) + d\bar{s} \sin(d\bar{\theta})}{2}$, an intrinsic description of this portion of the average curve. This averaging process is repeated for each pair of corresponding segments, $e.g.$, BC and $\bar{B}\bar{C}$. After combining each curve segment $(d\hat{s}, d\hat{\theta})$ the average curve is defined in an intrinsic form.

The averaging process in the general case of N curves is similar: compute the $d\hat{s}$ and $d\hat{\theta}$ by averaging $ds_i \cos(d\theta_i)$, and $ds_i \sin(d\theta_i)$. We have experimentally studied whether the choice of the "reference" curve affects the averaging process, and found that the averaging process is insensitive to this choice in our examples. In Figure 9, the averaging was repeated using each of the original curves as the textbook, and the average curve computed was more or less the same in all the cases.
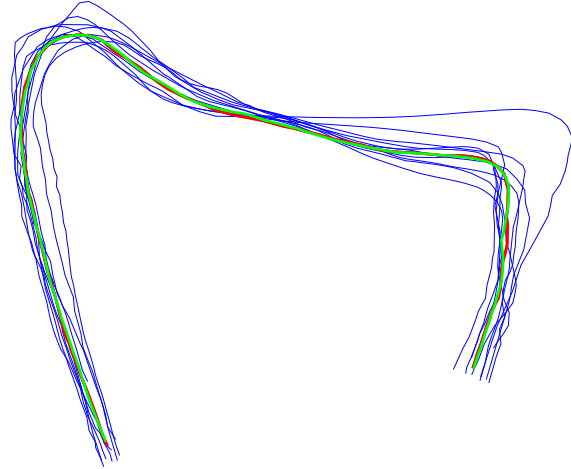

Figure 9. This figure illustrates the insensitivity of the average curve to the choice of the "reference" curve. The original curves are shown in blue. The averaging process is repeated by choosing two of the original curves as the "reference" curve and the result is shown in red and green.

We have applied the curve averaging algorithm to generate the average outline in a few medical imaging applications. Figures 7, 8 and 10 show the average outline computed from metacarpal bone outlines of thirteen subjects,
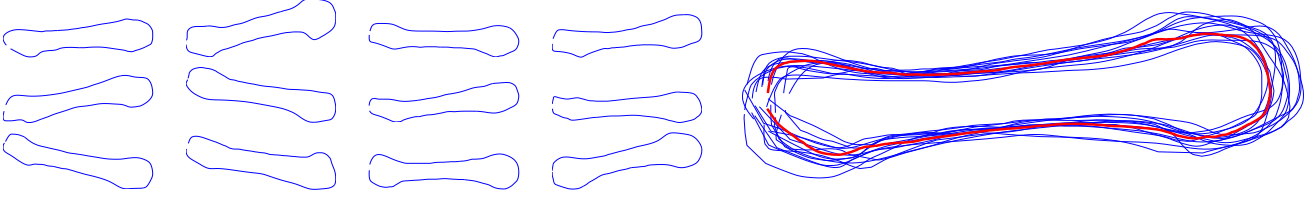
Figure 7. The average outline of the third metacarpal in the sagittal direction for twelve subjects is shown. The original bone contours are shown in blue, and the average outline in red. The bone contours were manually segmented from X-rays.
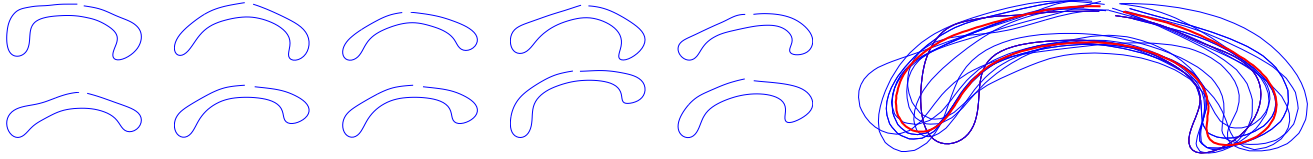

Figure 8. The average outline of the corpus callosum in the sagittal direction for ten is subjects is shown. The original corpus callosal outlines are shown in blue, and the average outline in red. The corpus callosal outlines were manually segmented from MR images. We thank Dr. James Eliassen and Prof. Jerome Sanes for providing us with the MR datasets.
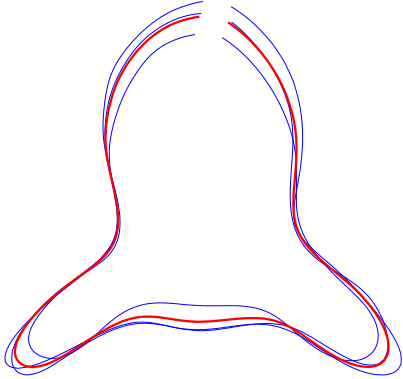

Figure 10. The average outline of a spine vertebra in the axial direction for three subjects is shown. The original outlines are shown in blue, and the average outline is depicted in red.

corpus callosal outlines from ten subjects, and the spine vertebra outlines of three subjects, respectively.

4 Curve Registration

In this section, we discuss how the curve matching framework is used to register 2D curves, $i.e.$, to recover the appropriate transformation (rotation and translation) parameters of one curve with respect to the other. A typical registration method computes these transformation parameters by minimizing a squared distance metric over all transformations. Let $\mathcal{C}$ and $\bar{\mathcal{C}}$ be the curves to registered, and let $(\bar{\mathcal{C}}^T : x_t, y_t, \theta_R)$ represent the transformed curve

$\bar{\mathcal{C}}$ after translation by (x_t, y_t) and rotation by θ_R. Let $D(\mathcal{C}, (\bar{\mathcal{C}}^T : x_t, y_t, \theta_R))$ be the squared distance between $\mathcal{C}$ and the transformed curve $\bar{\mathcal{C}}$. Typically the corresponding points are computed every iteration based on a pre-defined heuristic [13, 3]. For example, in [3] the corresponding points are defined to be the closest points. The optimal transformation parameters are computed as

$$\{x_t{}^{opt}, y_t{}^{opt}, \theta_R{}^{opt}\} = \operatorname*{argmin}_{x_t, y_t, \theta_R} D\left(\mathcal{C}, (\bar{\mathcal{C}}^T : x_t, y_t, \theta_R)\right)$$

(9)

We follow an alternate approach, namely, we first establish a transformation invariant correspondence between the two curves, and then recover the transformation parameters by minimizing the total squared distance between the corresponding points. The curve matching algorithm of Section 2 provides us with a such a correspondence between the two curves. Let $(x_i, y_i), i = 1, \ldots, N$ and $(\bar{x}_i, \bar{y}_i), i = 1, \ldots, N$ be the corresponding points on the two curves $\mathcal{C}$ and $\bar{\mathcal{C}}$, and $(\bar{x}_i^t, \bar{y}_i^t), i = 1, \ldots, N$ be the points on the transformed curve $\bar{\mathcal{C}}^T$. Then the distance between $\mathcal{C}$ and the transformed curve $\bar{\mathcal{C}}$ is given by

$$D(\mathcal{C}, (\bar{\mathcal{C}}^T : x_t, y_t, \theta_R)) = \sum_{i=1}^{N} \sqrt{(x_i - \bar{x}_i^t)^2 + (y_i - \bar{y}_i^t)^2}.$$

The minimization of the squared distance is done using the Levenberg-Marquardt method [14].

The optimal global scaling of the two curves is recovered in a similar fashion. Observe that the functional, Equation 5 that we used for curve matching is not scale-invariant (the
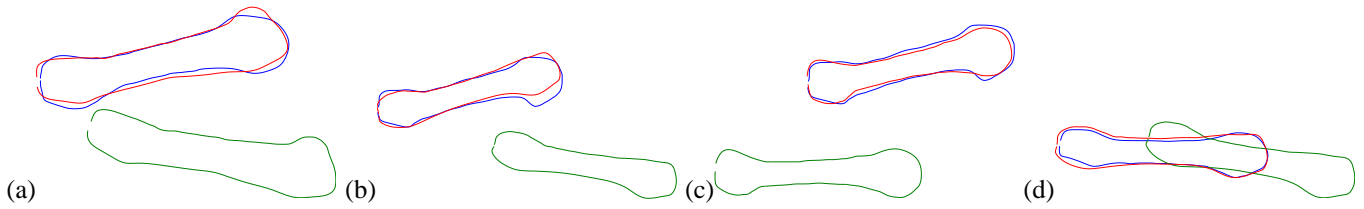
(a)   (b)   (c)   (d)

Figure 11. The third metacarpal bone contours from different subjects are used to illustrate the curve registration results. The bone contours were manually segmented from X-rays. Blue and green depict the contours that are to be registered, while the red depicts the optimal registration of the green curve to the blue curve.

bending term is scale invariant whereas the stretching term is not). Hence, if the second curve $\bar{\mathcal{C}}$ is scaled by λ the modified functional can be written as

$$\mu_\lambda[g] = \int_{\mathcal{C}} \left| \lambda \frac{d\bar{s}}{ds} - 1 \right| + R \left| \frac{d\bar{\theta}(\bar{s})}{ds} - \frac{d\theta(s)}{ds} \right| ds. \quad (10)$$

The optimal scaling factor λ^{opt} is then computed as $\underset{\lambda}{\arg\min}\, \mu_\lambda[g]$, which can be computed using gradient descent as $\mu_\lambda[g]$ is a convex function of λ. We note that only a small range of λ needs to be examined due to the one-norm used in defining μ.

We have used this approach to recover the transformation parameters for a few metacarpal outlines, Figure 11.

5   Comparing Average Curves

This section utilizes the curve averaging and registration methods described in the previous sections to examine if there are any differences in the average profiles of the radius bone between males and females. The average profile of ten male and female subjects in the sagittal and coronal directions were computed. The results, Figure 12, clearly show that there is a difference between the average profiles of males and female. However, it is not clear whether the differences are limited to size, $i.e.$, is the male profile a scaled up version of the female profile? To answer this question, we have computed the optimal transformation parameters (translation vector, rotation angle, and global scaling) between the average male and female profiles, have applied the optimal transformation, and examined whether the curves are aligned. The results Figure 12 that the differences are minimal. A more thorough and comprehensive analysis is required to quantify the differences between the profiles. The framework presented here provides a method for such analysis.

6   Conclusion

We have presented a method to compute the average of a set of 2D shape outlines (curves). We first compute an optimal, transformation invariant, alignment of two curves,

and then compute the average curve by averaging the corresponding curve segments. The alignment function between the curves is also be used to recover the optimal transformation parameters between the two curves. We have applied this method to a variety of medical images with excellent results.

References

[1] M. Bakircioglu, U. Grenander, N. Khaneja, and M. I. Miller. Curve matching on brain surfaces using induced Frenet distance metrics. *Human Brain Mapping*, 6(5):329–331, 1998.

[2] R. E. Bellman and S. E. Dreyfus. *Applied Dynamic Programming*. Princeton University Press, 1962.

[3] P. J. Besl and N. D. McKay. A method for registration of 3D shapes. *PAMI*, 14(2):239–256, 1992.

[4] F. Bookstein. Landmark methods for forms without landmarks: morphometrics of group differences in outline shape. *Medical Image Analysis*, 1(2):225–243, 1996/7.

[5] I. Cohen, N. Ayache, and P. Sulger. Tracking points on deformable objects using curvature information. *ECCV*, pages 458–466, 1992.

[6] T. A. Cormen, C. E. Leiserson, and R. L. Rivest. *Introduction to Algorithms*. McGraw Hill, 1989.

[7] C. Davatzikos, J. Prince, and R. Bryan. Image registration based on boundary mapping. *Trans. on Medical Imaging*, 15:212–215, 1996.

[8] J. Duncan, R. Owen, L. Staib, and P. Anandan. Measurement of non-rigid motion using contour shape descriptors. *CVPR*, pages 318–324, June 1991.

[9] D. Fritsch, S. Pizer, L. Yu, V. Johnson, and E. Chaney. Localization and segmentation of medical image objects using deformable shape loci. *IPMI*, pages 127–140. Springer 1230, 1997.
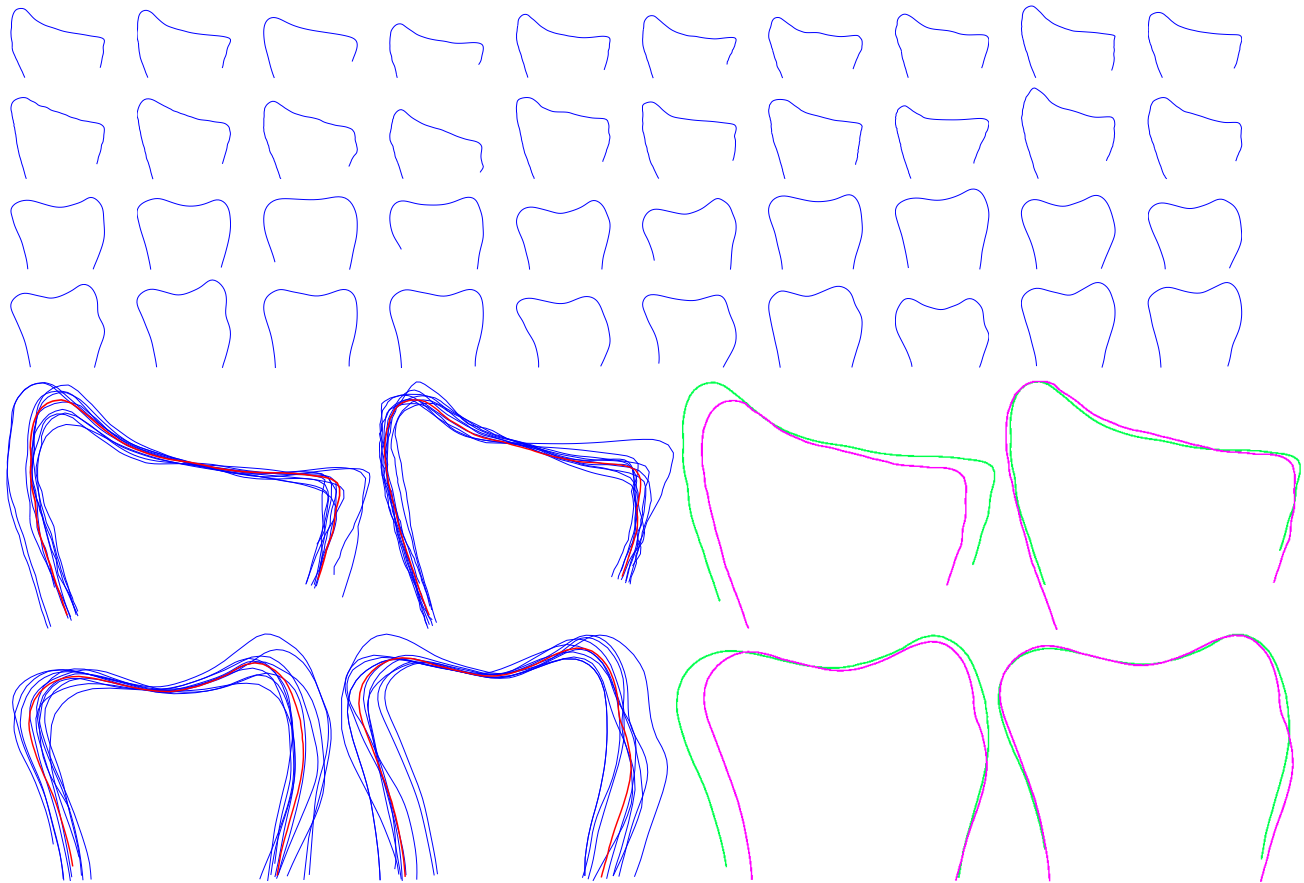
Figure 12. The profile of the radius in the sagittal direction for ten male (rows one and three) and ten female (rows two and four) subjects in sagittal (rows one and two) and coronal (rows three and four) directions. The average profile of the radius for ten sagittal sections (third row) and for ten coronal sections (fourth row) for ten males (first column of fifth row) and similarly for ten female subjects (second column of fifth row). The original profiles are shown in blue, and the average profile in red. The average profiles of male (green) and female (magenta) are then compared in the third column of the fifth and sixth rows. The average profiles of male (green) and female (magenta) are also compared after the optimal transformation (translation, rotation and scaling) is applied (last column of the fifth and sixth rows). This demonstrates that there are no significant differences between male and female radii except for size.

[10] U. Grenander and M. Miller. Computational anatomy: An emerging discipline. *Quarterly of Applied Mathematics*, LVI(4):617–694, 1998.

[11] M. Kass, A. Witkin, and D. Terzopoulos. Snakes: Active contour models. *IJCV*, 1:321–331, 1988.

[12] M. I. Miller, Y. Amit, G. E. Christensen, and U. Grenander. Mathematical textbook of deformable neuroanatomies. *Proc. of National Academy of Science*, 90(24), 1993.

[13] C. Pelizzari, G. Chen, D. Spelbring, R. Weichselbaum, and D. Levin. Accurate three-dimensional registration of CT, PET, and/or MR images of the brain. *J. Comp Assist Tomogr*, 13(1):20–26, 1989.

[14] W. Press, B. Flannery, S. Teukolsky, and W. Vetterling. *Numerical Recipes in C, 2nd ed.*, chapter Modeling of Data. Cambridge University Press, 1993.

[15] F. A. Schuind, R. L. Linsheid, K. An, and E. Chao. A normal database of posteroanterior roentgenographic measurements of the wrist. *The Journal of Bone and Joint Surgery*, 74-A(9):1418–1428, 1992.

[16] P. Smyth, C. Taylor, and J. Adams. Automatic measurement of vertebral shape using active shape models. *BMVC*, pages 9–12, 1996.

[17] H. Tagare, D. O'Shea, and A. Rangarajan. A geometric correspondence for shape-based non-rigid correspondence. *ICCV*, pages 434–439, 1995.

[18] L. Younes. Computable elastic distance between shapes. *SIAM Journal of Appl. Math.*, 1996.